

**Field
intercomparison**

B. Tuzson et al.

This discussion paper is/has been under review for the journal Atmospheric Measurement Techniques (AMT). Please refer to the corresponding final paper in AMT if available.

Field intercomparison of two optical analyzers for CH₄ eddy covariance flux measurements

B. Tuzson¹, R. V. Hiller², K. Zeyer¹, W. Eugster², A. Neftel³, C. Ammann³, and L. Emmenegger¹

¹Empa, Swiss Federal Laboratories for Materials Science and Technology, Laboratory for Air Pollution and Environmental Technology, Überlandstr. 129, 8600 Dübendorf, Switzerland

²ETH Zurich, Institute of Plant, Animal and Agroecosystem Sciences, Universitätsstr. 2, 8092 Zürich, Switzerland

³Agroscope Reckenholz-Tänikon Research Station ART, Reckenholzstr. 191, 8046 Zürich, Switzerland

Received: 10 June 2010 – Accepted: 22 June 2010 – Published: 13 July 2010

Correspondence to: B. Tuzson (bela.tuzson@empa.ch)

Published by Copernicus Publications on behalf of the European Geosciences Union.

Title Page

Abstract

Introduction

Conclusions

References

Tables

Figures

◀

▶

◀

▶

Back

Close

Full Screen / Esc

Printer-friendly Version

Interactive Discussion



Abstract

Fast response optical analyzers based on laser absorption spectroscopy are the preferred tools to measure field-scale mixing ratios and fluxes of a range of trace gases. Several state-of-the-art instruments have become commercially available and are gaining in popularity. This paper aims for a critical field evaluation and intercomparison of two compact, cryogen-free and fast response instruments: a quantum cascade laser based absorption spectrometer from Aerodyne Research, Inc., and an off-axis integrated cavity output spectrometer from Los Gatos Research, Inc. In this paper, both analyzers are characterized with respect to precision, accuracy, response time and also their sensitivity to water vapour. The instruments were tested in a field campaign to assess their behaviour under various meteorological conditions. The instrument's suitability for eddy covariance flux measurements was evaluated by applying an artificial flux of CH₄ generated above a managed grassland with otherwise very low methane flux. This allowed an independent verification of the flux measurements accuracy, including the overall eddy covariance setup and data treatment. The retrieved fluxes were in good agreement with the known artificial emission flux, which is more than satisfactory, given that the analyzers were attached to separate sonic anemometers placed on individual eddy towers with different data acquisition systems but similar data treatment that are specific to the best practice used by the involved research teams.

1 Introduction

Understanding the temporal dynamics of methane emission and its relationship to environmental drivers at global scale requires continuous and long-term measurements of CH₄ fluxes at the landscape level (Bartlett and Harriss, 1993; Bubier and Moore, 1994). The well established chamber technique, however, poorly captures the spatial and temporal variability of gas exchange despite its undebated usefulness for small scale (plot-level) studies. The general problems associated with chamber flux

AMTD

3, 2961–2993, 2010

Field intercomparison

B. Tuzson et al.

Title Page

Abstract

Introduction

Conclusions

References

Tables

Figures

◀

▶

◀

▶

Back

Close

Full Screen / Esc

Printer-friendly Version

Interactive Discussion



**Field
intercomparison**

 B. Tuzson et al.

[Title Page](#)
[Abstract](#)
[Introduction](#)
[Conclusions](#)
[References](#)
[Tables](#)
[Figures](#)
[◀](#)
[▶](#)
[◀](#)
[▶](#)
[Back](#)
[Close](#)
[Full Screen / Esc](#)
[Printer-friendly Version](#)
[Interactive Discussion](#)


measurements are leaks, inhibition of fluxes through concentration build-up and pressure effects, which are well known limitations of this method (Matthias et al., 1978; Bain et al., 2005; Camarda et al., 2009). Alternatively, micrometeorological methods like eddy covariance (EC) integrate trace gas exchange over extended areas (typically tens of m²) – appropriate for landscape scale studies. However, these techniques rely on fast response, field-deployable and high-sensitivity instruments, which can rapidly resolve small (preferably better than 0.1%) concentration changes in CH₄ at ambient level. Until recently, EC flux measurements of CH₄ required frequent re-calibration and/or liquid nitrogen for the analyzers (Verma et al., 1992; Fowler et al., 1995; Friborg et al., 1997; Werle and Kormann, 2001) leading to logistic limitations for unattended field deployment.

Recently, a number of new instruments appeared on the market, which may overcome these shortcomings. However, just a very few studies have addressed their application in the field for EC flux measurements and they focus on only one single type of analyzer (Eugster et al., 2007; Neftel et al., 2007; Kroon et al., 2007; Hendriks et al., 2008; Smeets et al., 2009; Eugster and Plüss, 2010). For novel instruments, it is rather challenging to validate the retrieved EC flux data, because one cannot rely on a reference method, and CH₄ emissions of natural sources are often very small. Although the analyzers may give the correct concentration under laboratory conditions, these readings do not necessarily translate to a representative surface fluxes during a field campaign.

Here we propose to characterize and compare two cryogen-free optical analyzers that allow for fast and high precision measurement of methane mixing ratios in ambient air. For the validation of flux data during field deployment, an artificial methane flux was generated above an intensively managed grassland with otherwise very low methane flux. To our knowledge, this is the first example of an intercomparison for methane flux measurements where eddy covariance CH₄ flux data were validated against a known, artificial source.

2 Material and methods

2.1 Instrumentation

In this study, we investigated two commercially available optical analyzers that are cryogen-free and allow for CH₄ measurements at high (>10 Hz) temporal resolution: 1) an off-axis integrated-cavity output spectrometer (Model 908-0001, Fast Methane Analyzer, Los Gatos Research Inc., Mountain View, CA) and 2) a dual continuous wave (cw) quantum cascade laser based direct absorption spectrometer (Model QCL-76-D, Aerodyne Research Inc., Billerica, MA). Even though the optical implementation and the signal processing techniques used in the two instruments are quite different, the underlying principles of infrared (IR) absorption spectroscopy apply to both analyzers. The trace gas mixing ratios are determined based on the Beer-Lambert law:

$$\ln(I_0/I) = k_\nu nL = S_i \phi_\nu nL \quad (1)$$

which relates the attenuation of light (I and I_0 being the transmitted and incident light intensity, respectively) to the particle density n [molecule/cm³] of absorbing molecules along the light path of length L [cm]. In this equation k_ν [1/(molecule cm⁻²)] denotes the spectral absorption coefficient for an isolated transition i , and it is defined by the line strength of the transition S_i [cm⁻¹/(molecule cm⁻²)] and by the normalized line shape function ϕ_ν [1/cm⁻¹]. The number density, n , can easily be expressed in mole fraction of the absorbing species using the ideal gas law. Given that the minimum still-detectable concentration is determined by the noise-equivalent-power, absorption path length, absorption cross section and the incident laser power, it is evident that the detection sensitivity can be optimized using several approaches.

The quantum cascade laser based absorption spectrometer (QCLAS) employs a mid-IR quantum cascade laser as light source which is particularly attractive due to its stable single mode spectral output, high power and near room temperature operating condition. The advantage of selecting the mid-IR spectral region is that the majority of trace gas molecules of interest have their fundamental ro-vibrational absorption bands

Title Page

Abstract

Introduction

Conclusions

References

Tables

Figures

◀

▶

◀

▶

Back

Close

Full Screen / Esc

Printer-friendly Version

Interactive Discussion



**Field
intercomparison**

B. Tuzson et al.

Title Page

Abstract

Introduction

Conclusions

References

Tables

Figures

◀

▶

◀

▶

Back

Close

Full Screen / Esc

Printer-friendly Version

Interactive Discussion



located at these energies and therefore the absorption strengths are also the highest here. This explains the ability of the analyzer, equipped with two lasers, to measure not only CH₄ and H₂O, but also the mixing ratios of N₂O and NO₂, respectively (see Table 1). For this study, however, only the CH₄ and H₂O data were considered. The signal-to-noise ratio (SNR) is significantly improved by employing a multipass absorption cell which increases the effective light path through the absorber by more than two orders of magnitude. Nevertheless, the main challenge in the direct absorption approach is to accurately measure small changes ($\Delta I = I_0 - I$) of two large quantities. This limitation can be overcome by the rapid sweep integration technique, where the absorption spectrum is typically acquired at 5–10 kHz and the co-addition of many individual scans results in rapid gains in SNR. Optical fringes mainly resulting from unwanted etalons formed by reflections and scattering in the multipass cell are effectively suppressed by a proper mechanical modulation of the cell's rear mirror using a piezo-crystal (McManus et al., 2006).

The Fast Methane Analyzer (FMA), on the other hand, operates in the near-IR region where low-cost distributed feedback diode laser sources as well as photodetectors with high detectivity values are readily available, and fibre optics can be efficiently used. This results in very compact, robust and easy-to-build systems. However, the absorption strength (overtone transitions) of the molecules is 10 to 10³ times weaker than in the mid-IR region. To circumvent this constraint, a high-finesse optical cavity with high reflectivity mirrors ($R > 0.9999$) is used to achieve an effective path length of light on the order of kilometers (see Table 1). Thus, the laser beam is trapped for tens of microseconds. The absorption signal is obtained in this case by the time integrated intensity of the light passing through the cavity with and without the absorbing medium and expressed as:

$$\Delta I / I_0 = GA / (1 + GA) \quad (2)$$

where A is the single-pass absorption [$A = 1 - \exp(-k_v d)$] and $G = R / (1 - R)$. R is the mirror reflectivity, and d is the interaction length of the laser beam with the absorbing

medium. Once the mirror reflectivity is determined from a known concentration standard, it also serves for the absolute calibration of the FMA.

For both analyzers, the absorption features are fitted to a Voigt profile, and the concentrations are retrieved based on measured pressure, temperature, path length and molecular parameters, which are listed in spectral data-bases such as HITRAN (Rothman et al., 2009). While the FMA is stated to be calibrated by the manufacturer, the QCLAS requires calibration by the user. More detailed descriptions of the instrumental design and signal processing have been published by Nelson et al. (2002) for QCLAS and by Baer et al. (2002) for FMA, respectively.

2.2 Measurement site

The field measurements were conducted at the Oensingen experimental site, which is located on the Swiss Plateau (7°44' E, 47°17' N) at an altitude of 450 m a.s.l. The managed grassland field is part of the global FLUXNET observation network and the two large integrated European projects CarboEurope and NitroEurope (Ammann et al., 2007). All experiments assessing the analyzers performance were performed in this field site, which was motivated by our effort to test the instruments under the same conditions as they are employed in the EC measurements. The only exception was the water dilution experiment, which required, as it will be discussed in Sect. 3.1.3, a temperature-controlled laboratory environment for an accurate water vapour generation and consecutive measurements by the analyzers.

2.3 Trace gas flux generation

An objective evaluation of the suitability and accuracy of the instruments for measuring methane fluxes by the EC method was achieved by an artificial flux generation system, which mimics an amplified ecosystem-atmosphere gas exchange. For this purpose, stainless steel tubing of 1/4" outer diameter was used to construct a rectangular grid containing 30 flow orifices (30 µm, Lenox Laser, USA) as gas outlets. As illustrated in

Field intercomparison

B. Tuzson et al.

Title Page

Abstract

Introduction

Conclusions

References

Tables

Figures

◀

▶

◀

▶

Back

Close

Full Screen / Esc

Printer-friendly Version

Interactive Discussion



Fig. 1, the grid consisted of three parallel lines of 30 m length, 5 m apart to approximate a surface area of 300 m². Each line embodied 10 flow orifices placed every 3 m along the tubing to obtain an even release of trace gas across the fumigation area.

The gas release experiment took place in two periods between 25–29 March (south-westerly wind directions, see Fig. 1) and 30 March–6 April 2009 (north-easterly wind directions). For the first period, the trace gas was obtained through continuous dilution of pure CH₄ with N₂ to a concentration of 5%, while during the second period, a pressurized cylinder (40 L, Messer, Switzerland) containing 1% mole fraction of methane in pure N₂ was coupled to the manifold through a pressure regulator. The trace gas mixture was continuously released at a rate of 0.8 L min⁻¹ set by a mass flow controller (Vögtlin Instruments, Switzerland) at an overpressure of 1.8 atm.

To relate the area of the artificial flux to the area seen by the measuring system, the footprint of the flux measurements was calculated according to Neftel et al. (2008). The calculations are based on the analytical footprint model by Kormann et al. (2001). The footprint density function of a flux sensor is determined using readily available data from the standard eddy covariance measurements. This footprint density function is then integrated over the fumigation source area given as quadrangular polygon (Fig. 1). Its fraction gives the dilution factor of the measured flux in relation to average emission flux in the source area.

2.4 Flux measurements

During the field measurements, the FMA was placed in a weatherproof housing close to the eddy flux tower, whereas the QCLAS was kept in an air-conditioned (23±2 °C) trailer to minimize temperature fluctuations. Additionally, the entire optical module of the QCLAS was insulated and the baseplate as well as the cover were maintained at 35±0.1 °C. A constant flow of dry air purged the optics to prevent condensation, which may occur due to the low temperature (16 °C) of the cooling water used for the QCL and the IR-detectors. The trailer was located about 25 m away from the eddy flux tower in crosswind direction. The instrument automatically switched between ambient air

Field intercomparison

B. Tuzson et al.

Title Page

Abstract

Introduction

Conclusions

References

Tables

Figures

◀

▶

◀

▶

Back

Close

Full Screen / Esc

Printer-friendly Version

Interactive Discussion



(four hours) and calibration gas (two minutes). The FMA ran without any calibration procedure.

For the flux measurements, each trace gas analyzer was connected to separate sonic anemometers, thus forming two individual eddy flux systems (see Table 1). The two systems (sonic and sample air inlets) were mounted close to each other at a lateral distance of 0.7 m. In addition, CO₂ and H₂O fluxes were routinely measured with another EC system on the same field (Ammann et al., 2007) positioned at a distance of about 7 m. In order to obtain a large overlap between the size of the flux footprint and the CH₄ fumigation area, the measurement height of the EC systems was chosen relatively low at 1.2 m above ground.

For the EC flux measurements, the FMA was connected to an external vacuum scroll pump (XDS-35i BOC, Edwards) with a maximum pumping capacity of 580 L min⁻¹. The sample was drawn through 6.7 m long tubing (8 mm i.d.) followed by two serially mounted filters (5 μm and 0.3 μm, respectively) with droplet separator. The FMA has a pressure controller that throttles the flow to maintain the cell at its target pressure of ≈19 kPa. Due to the pressure drop within the sampling system and analyzer, the pumping speed was reduced to an effective gas flow of about 30.5 sL min⁻¹.

The QCLAS was connected to a scroll pump (TriScroll 600, Varian) with a maximum pumping capacity of 420 L min⁻¹. As the QCLAS has no built-in pressure or flow control system, it is left to the user to deal with these issues. In the present study, a mass flow controller regulated the gas flow into the absorption cell, while a high-flow throttle valve was used to provide manual control of the downstream flow to keep the cell pressure at about 8 kPa. Since the analyzer was placed in a trailer 25 m away from the eddy flux tower, a custom made sampling tube (6 mm i.d., Hot Tube, Clayborn Lab, USA) was used to conduct the air stream to the instrument. The air sample was first filtered at the inlet by a Teflon membrane filter (slightly heated by thermofoil elements) and secondly before entering the absorption cell using a 7 μm sintered metal filter (Swagelok). The sampling tubing was maintained at about 10 °C above ambient temperature by applying a constant current through its heating elements. The air was dried using a Nafion drier

**Field
intercomparison**

B. Tuzson et al.

Title Page

Abstract

Introduction

Conclusions

References

Tables

Figures

◀

▶

◀

▶

Back

Close

Full Screen / Esc

Printer-friendly Version

Interactive Discussion



(PD-100T, Perma Pure, USA) just before the analyzer. This setup resulted in a turbulent flow of 13.5 sL min^{-1} .

More details about the EC setups and data processing methods are given by Eugster and Plüss (2010) and Neftel et al. (2010) for the FMA and QCLAS setup, respectively.

5 In contrast to Eugster and Plüss (2010), the methane signal of the FMA system was linearly detrended prior to the flux calculations to be consistent with the data processing strategy of the QCLAS EC system.

3 Results and discussion

10 In this section, we first present the results of the analyzers' performance tests and discuss the various effects which may influence the retrieved mixing ratio values. Then, in situ methane concentration measurements and CH_4 flux determination of the artificially fumigated area will be discussed. Finally, we compare the experimentally determined fluxes with the known emissions of the fumigation area.

3.1 Instrument characterisation

15 3.1.1 Precision

The instrument performance in terms of detection limit and long-term stability was characterized in the field by the Allan variance technique (Werle et al., 1993). For this purpose, the analyzers were connected through a T-split to a pressurized air cylinder and they measured the same dry gas over 16 h. The gas flow rate was 2 L min^{-1} and the analyzers were configured for low flow mode, but maintaining the same cell pressure as in the high-flow mode used for EC measurements (see Table 1). The total gas consumption of the analyzers was 1.28 L min^{-1} , while the rest was released through an overflow. The methane mixing ratio was measured with a time resolution of one second. The precision was 1 and $3 \text{ ppb Hz}^{-1/2}$ for FMA and QCLAS, respectively (Fig. 2).

Field intercomparison

B. Tuzson et al.

Title Page

Abstract

Introduction

Conclusions

References

Tables

Figures

◀

▶

◀

▶

Back

Close

Full Screen / Esc

Printer-friendly Version

Interactive Discussion



**Field
intercomparison**

B. Tuzson et al.

[Title Page](#)[Abstract](#)[Introduction](#)[Conclusions](#)[References](#)[Tables](#)[Figures](#)[◀](#)[▶](#)[◀](#)[▶](#)[Back](#)[Close](#)[Full Screen / Esc](#)[Printer-friendly Version](#)[Interactive Discussion](#)

From the associated Allan variance plots an optimum averaging time on the order of 500 s can be derived. This corresponds to a detection precision of 0.23 and 0.58 ppb, respectively. For integration times beyond 500 s, the Allan variance levels off and even increases, which indicates the presence of $1/f$ -type and “drift” noise. It is noteworthy that the Allan variance may have significant variations in time. This behaviour is indicated in Fig. 2 where the range defined by many individual 30 min Allan plots is shown (shaded area). Such representation illustrates that it is always possible to obtain “nice” Allan plots with low drift, and hence good precision, by selecting the best data segment from an extended time series. Figure 2 also shows that for half hour averaging (commonly used in EC techniques) the advantage of the FMA’s higher short-time precision is somewhat diminished by low frequency instrumental drifts.

The Allan variance plots in Fig. 2 are typical in the sense that they contain frequency independent white noise and frequency dependent $1/f^\alpha$ ($\alpha > 1$) noise (Werle et al., 1993). The latter encompasses a noise at low frequencies which can be considered as drift. Accordingly, the Allan variance has a characteristic “V-shape” defined by the white-noise dominated region at short integration times and by the domain of various drift effects at longer integration times. Our results are consistent with other recent work (Kroon et al., 2007; Smeets et al., 2009; Eugster and Plüss, 2010; Bowling et al., 2009), suggesting that the achievable detection limit for methane with the existing analyzers is about 1 to 5 ppb $\text{Hz}^{-1/2}$, which implies that variations of 0.05% in ambient methane concentration are readily captured. The only strikingly different Allan variance plot has recently been published by Hendriks et al. (2008). This plot has no clear domains nor local minima, and the reported precision (6.1×10^{-3} ppb $\text{Hz}^{-1/2}$) is at least two orders of magnitude better than what is expected from the stated precision (4.74 ppb) at a sampling rate of 10 Hz. Assuming a pure white-noise behaviour of the analyzer, the estimated precision should rather be $4.74/\sqrt{10}$ or 1.5 ppb $\text{Hz}^{-1/2}$.

3.1.2 Accuracy

In principle, direct absorption spectroscopy is an absolute method that should allow for a straightforward calculation of the concentration from the measured signals. However, the accuracy of this calculation depends on the knowledge of the molecular line parameters including line strength, pressure and temperature dependence (listed in the spectral databases), as well as instrumental laser line width and shape. Additionally, non-unity gain factors and potential cross-coupling effects also bias the retrieved mixing ratios. Whereas the FMA is delivered with factory calibration, the QCLAS is shipped without calibration, and all corrections need to be performed by the user during a post processing step.

Three reference gases were used to determine the accuracy and the linearity of the analyzers and to calibrate the QCLAS. One cylinder (1838.5 ± 0.3 ppb CH_4) was prepared and calibrated at the National Oceanic and Atmospheric Administration/Climimate Monitoring and Diagnostics Laboratory (NOAA/CMDL), while the other two (2273.1 ± 0.5 ppb and 2478.8 ± 0.5 ppb, respectively) were secondary standards linked to the CMDL scale. A four-point calibration (including zero) was performed, but given the stability and linearity of the analyzers a two point calibration would be sufficient. The calibration factor was 1.0003 and 1.0516 for FMA and QCLAS, respectively. The reproducibility determined by replicate measurements of the target tank was 0.9 ppb for FMA and 1.7 ppb for the QCLAS. It is noteworthy that the excellent accuracy of the FMA has been maintained even after transport and under field deployment.

3.1.3 Response to water vapour

It is well known that density fluctuations arising from heat and water vapour fluxes affect the measured flux densities of trace gases according to the Webb-Pearman-Leuning (WPL) theory (Webb et al., 1980). The following paragraphs are dealing with considerations related to water vapour that are not directly covered by the WPL theory, such as the effect of water vapour on the spectral line shape. Drying the air sample or

AMTD

3, 2961–2993, 2010

Field intercomparison

B. Tuzson et al.

Title Page

Abstract

Introduction

Conclusions

References

Tables

Figures

◀

▶

◀

▶

Back

Close

Full Screen / Esc

Printer-friendly Version

Interactive Discussion



measuring its absolute moisture content is required for an accurate methane mole fraction determination. This is, because the laser spectrometers measure the mixing ratio of CH₄ to total pressure (P_t), including also the vapour partial pressure ($P_w=[H_2O]P_t$), whereas the methane concentration in calibration gas is defined as *dry air mole fraction*. A dilution correction must thus be applied to the reported raw mixing ratio values

$$[CH_4]_{dry}=[CH_4]_{wet}P_t/(P_t-P_w) \quad (3)$$

Furthermore, changing the gas composition by varying its water content will influence the spectral line shape of the absorbing molecule (in this case CH₄) due to the collisional broadening effect and thus, the derived mixing ratio value. As the line shape function (see Eq. 1) is determined by the physical mechanisms that perturb the energy levels of the transition (Varghese and Hanson, 1984), it is obvious that perturbations caused by molecular collisions may differ as a function of the colliding molecules type. Within the binary collision assumption the collisional broadening effect is introduced as a Lorentz function with a full-width at half maximum (γ_c) that is proportional to the sample pressure

$$\gamma_c = \sum_j \gamma_j P_j \quad (4)$$

where γ_j (cm⁻¹ atm⁻¹) is the transition dependent broadening coefficient quantifying the ability of a molecular species j (e.g. N₂, O₂, and H₂O) from the air sample to cause pressure broadening due to the collisions with the absorbing molecules. The role of this collision-induced interference of spectral lines in ro-vibrational spectroscopy is in many cases underestimated. It is often stated that the instruments are interference free, which, however, only means that there is no spectral overlap between the absorption line of the trace gas of interest and the absorption features of other molecular species. Therefore, one might misleadingly assume that there is no cross-sensitivity to other ambient air species. Nevertheless, this assumption should be investigated carefully in the case of trace gas flux measurements, because water vapour concentrations

**Field
intercomparison**

B. Tuzson et al.

Title Page

Abstract

Introduction

Conclusions

References

Tables

Figures

◀

▶

◀

▶

Back

Close

Full Screen / Esc

Printer-friendly Version

Interactive Discussion



**Field
intercomparison**

B. Tuzson et al.

[Title Page](#)
[Abstract](#)
[Introduction](#)
[Conclusions](#)
[References](#)
[Tables](#)
[Figures](#)
[◀](#)
[▶](#)
[◀](#)
[▶](#)
[Back](#)
[Close](#)
[Full Screen / Esc](#)
[Printer-friendly Version](#)
[Interactive Discussion](#)


can vary rapidly and are often correlated with vertical wind speed. Thus, any cross-sensitivity of trace gases to water may lead to an apparent flux. In principle, it would be possible to implement in the retrieval software an algorithm to account for this collision-induced effect based on the theory of pressure broadening. However, the commonly used spectral database, HITRAN, contains only the dry air broadened half-width (γ_{air}) for most of the absorption lines (Brown et al., 2003). Investigations performed on simulated spectra which included the pressure broadening effect showed that quantification using least-square fit of a Voigt profile will systematically underestimate the mixing ratio values. For ambient water vapour level ($<4\%$ v), the magnitude of this underestimation can be well approximated using a linear dependence on the vapour partial pressure, and thus a simple cross-sensitivity correction can be applied to the measured CH_4 concentration:

$$[\text{CH}_4] = [\text{CH}_4]_{\text{dry}} + b_{\text{ct}} P_w / P_t \quad (5)$$

where b_{ct} is the cross-talk coefficient of the particular device (Neftel et al., 2010), which can also be determined empirically as shown below. Before doing so, we should mention an important aspect regarding the above corrections. While the dilution effect depends only on the absolute amount of water vapour in the air sample, i.e. it is always present in humid air sample, the water pressure broadening causing the cross-talk effect will linearly depend on the concentration of the absorbing trace gas. This has an impact on the determination of the b_{ct} value. For example, the slope will be twice as steep when the concentration of the absorbing trace gas is doubled, but it vanishes as the concentration approaches zero.

To investigate the effect of increasing humidity on the retrieved CH_4 concentration, the analyzers were installed in an air conditioned laboratory and measured the gas from a pressurized dry air cylinder coupled to a water vapour generation system (LI-610, LI-COR Inc., USA). This dew-point generator gradually increased the humidity level of the gas every 20 min. The QCLAS simultaneously measured the methane concentration and the water vapour in the humidified samples. Thus, every single CH_4 concentration measurement can be normalized to dry conditions (see Eq. 3) given that

**Field
intercomparison**

B. Tuzson et al.

Title Page

Abstract

Introduction

Conclusions

References

Tables

Figures

◀

▶

◀

▶

Back

Close

Full Screen / Esc

Printer-friendly Version

Interactive Discussion



the humidity data are calibrated. The LI-610 has been considered as reference point for absolute water concentration. The results of the water dilution experiment are shown in Fig. 3. It clearly indicates that correcting for dilution by water vapour only is not sufficient and, because no direct spectral interference to water vapour is expected in this spectral region, the observed behaviour is attributed to the line broadening effect of the increasing water content in the gas-matrix (Neffel et al., 2010). Moreover the effect shows, in accordance with the theoretical prediction, a clear dependence on the water vapour, which although is non-linear, it still can be approximated by a linear function at usual ambient water vapour concentrations (<4%v). In our case its magnitude is about 16% of the density correction, but as mentioned earlier, the exact value depends on the CH₄ concentration as well as on the absorption lines which are used to retrieve the mixing ratios. In this context, it is rather a coincidence that both analyzers showed exactly the same cross-talk effect, because the absorption lines analyzed by the instruments are located at different (near and mid-IR, respectively) spectral regions. In contrast to the QCLAS, the FMA measures a spectral feature of CH₄ that is a combination of four individual, but closely spaced, and thus not resolved, absorption lines (see Table 1). Nevertheless, this empirical approach allows for the determination of the cross-talk coefficient b_{ct} without the knowledge of the water pressure broadening coefficient value.

We also tried to repeat the dilution experiment in the field by gradually adding water vapour to the gas stream from a pressurized air cylinder as described by Neffel et al. (2010), but in this case the FMA showed only a random response to the increased humidity. One could only speculate about the nature of such instability. We associated this phenomenon with the presence of two serially mounted filters (5 μm coarse filter followed by 0.3 μm fine filter) both with droplet separators attached to the FMA for further protection of the cell mirrors during the field campaign.

To summarize, the dilution experiment gives us a solid evidence that water vapour flux may introduce an apparent methane flux similar to the water vapour density effect. This apparent CH₄ flux is most significant for small but real CH₄ fluxes and large water

vapour fluxes. In the density flux correction equation proposed by Webb et al. (1980) there are three terms:

$$F = \underbrace{\overline{w'\rho'_c}}_I + \underbrace{\mu \left(\overline{\rho_c/\rho_a} \right) \overline{w'\rho'_v}}_{II} + \underbrace{(1 + \mu\sigma) \left(\overline{\rho_c/T} \right) \overline{w'T'}}_{III}, \quad (6)$$

where w is vertical wind speed in m s^{-1} , ρ_c , ρ_a , and ρ_v are the densities of gas c , air, and vapour, respectively, in kg m^{-3} , T is air temperature in K, and $\mu = m_a/m_v$ and $\sigma = \overline{\rho_v/\rho_a}$. m_a and m_v are the molar masses (“weights”) of dry air and water vapour, respectively, in kg mol^{-1} . Term (I) is the measured flux, term (II) is the moisture flux correction, and term (III) is the sensible heat flux correction. Since temperature fluctuations are largely under control in a closed-path CH_4 analyzer such as the ones used here, this term becomes negligibly small and hence we will focus on term (II). This term is non-negligible if water vapour is not removed from the air stream prior to analysis. As shown by Neftel et al. (2010), the water cross sensitivity on CH_4 can formally be treated similar to the density correction. Its influence increases linearly with the water flux and will consequently be most pronounced in summer conditions with high transpiration of the plant canopy. This effect is illustrated by a series of measurements over the same grassland field taken in August 2008, using the same QCLAS setup, but without drying the air samples. Consequently both, the density (WPL) and the cross interference corrections had to be applied. This was performed numerically on the individual 20 Hz raw data values. This procedure avoids the potential overestimation of the correction due to the fact that the residence time of water molecules in the sampling line is slightly longer than that of non polar molecules such as CH_4 (Ibrom et al., 2007). Figure 4 shows the scatter plot of the evaluated CH_4 EC fluxes at different stages of corrections. The corrected fluxes have been evaluated with a prescribed lag that was derived from the maximum of the covariance function of the non corrected fluxes. This lag corresponds to the expected time delay based on the tube length, diameter and pump speed. The strong negative apparent CH_4 fluxes up to $-15 \text{ nmol m}^{-2} \text{ s}^{-1}$ are evidently induced by water vapour fluxes, because the CH_4 exchange fluxes of the grassland

Field
intercomparison

B. Tuzson et al.

Title Page

Abstract

Introduction

Conclusions

References

Tables

Figures

◀

▶

◀

▶

Back

Close

Full Screen / Esc

Printer-friendly Version

Interactive Discussion



system in Oensingen are expected to be very small. Applying the density corrections reduces these negative fluxes to $-5 \text{ nmol m}^{-2} \text{ s}^{-1}$. However, this still exceeds plausible limits of CH_4 uptake fluxes (Neftel et al., 2010; Smith et al., 2000). The second correction brings the CH_4 fluxes to slightly positive values that are individually not significantly different from zero, but do show a tendency to small emission fluxes, correlated with the water vapour flux. These positive values are above the highest emission fluxes that can be expected based on reports in the literature (Keppler et al., 2006), and are fully dominated by the uncertainties in the applied correction factors (water calibration of the QCLAS, cross interferences of the water concentration on the CH_4 concentration) and is sensitive to any slight change in these factors.

Although not considered in this study, it should still be mentioned that an additional effect may also influence the final CH_4 flux values. This effect has its origin in the well known physical process of adsorption of gas molecules on solid surfaces predominantly due to attractive Van der Waals forces. In the classical model of gas adsorption (Langmuir's model) it is assumed that gas molecules striking the surface have a given probability of becoming adsorbed, while molecules already adsorbed similarly have a given probability of desorbing, which leads to a dynamic equilibrium where the average number of molecules per unit area of surface per time interval are constant. The accumulation of a specific molecule on a solid surface is influenced by many factors involved in the interactions between the solid surface, water and the species concerned. This also means that there is a possibility that trace gases like CH_4 could be influenced by changes in the air humidity due to the competitive sorption of water vapour on the surface. Given that water molecules have a high potential to replace other molecules from surfaces and variation in the water vapour concentrations in high flux conditions are on the order of 10%, i.e. about 5 orders of magnitude higher than the expected CH_4 variations, it may be worthwhile to consider this effect in future investigations.

**Field
intercomparison**

B. Tuzson et al.

Title Page

Abstract

Introduction

Conclusions

References

Tables

Figures

◀

▶

◀

▶

Back

Close

Full Screen / Esc

Printer-friendly Version

Interactive Discussion



3.1.4 Influence of temperature and pressure

The QCLAS is rather sensitive to ambient temperature fluctuations. This is due to the relative large number of optical elements and the thermoelectrically cooled (TEC) infrared detectors (Vigo Systems, PL). As mentioned in Sect. 2.1, the SNR can be strongly influenced by optical fringes whose magnitude mainly depends on the alignment accuracy of the optical system. Furthermore, the employed detectors are particularly sensitive to the aiming angle of incident light. This is due to the small size of the photodiodes (0.5 mm² active area) and to their optical immersion into high refractive index GaAs hyperhemispherical lenses. The influence of the changes in the optical aiming on the measured CH₄ mixing ratio was empirically estimated by deliberately creating a misalignment which caused 5% decrease in the laser intensity on the detector. This resulted in an apparent change of 23 ppb CH₄. Considering the laser intensity variations of about 0.35% over many hours during the field campaign, the noise contribution to the analyzer precision was about 1.6 ppb at most.

The influence of changing cell temperature and pressure on the measured methane concentration by FMA has also been investigated. Even though the analyzer showed an excellent stability during the field test, it was not completely immune to changes in ambient conditions and a temperature dependence of 0.84 ppb K⁻¹ could be established. Additionally, the CH₄ concentration values systematically dropped by 51 ppb when switching from low to high flow mode. This, however, has no influence on typical eddy covariance measurements.

3.1.5 Response time

In order to evaluate their responsiveness, the analyzers were placed in the field in their typical sampling configuration as used for the eddy-covariance flux measurements. The FMA sample gas flow of about 30.5 sL min⁻¹ corresponds to 165 L min⁻¹ gas flow at a nominal cell pressure of 19 kPa. Thus, the cell volume of 0.408 L is refreshed at approximately every 0.15 s. In this configuration the data acquisition was set to 20 Hz.

Title Page

Abstract

Introduction

Conclusions

References

Tables

Figures

◀

▶

◀

▶

Back

Close

Full Screen / Esc

Printer-friendly Version

Interactive Discussion



For the QCLAS system, the sample flow of 13.5 sL min^{-1} corresponds to 171 L min^{-1} at a nominal cell pressure of 8 kPa. Thus, the cell volume of 0.5 L is refreshed at approximately every 0.18 s. To be consistent with this physical response time, the spectral retrieval rate was set to 8 Hz, although data acquisition rates of up to 20 Hz would have been possible.

The above reported values for the cell refresh rate were calculated based on the cell volume divided by the actual pumping speed. The real response time (first order, $1/e$) was also empirically determined in the field, through the entire sampling setup, by rapidly switching from ambient air to calibration gas and fitting the rising/falling tail to an exponential function. The instrumental response (0.23 s for QCLAS and 0.4 s for FMA) of this empirical approach is slightly slower than expected based on the well-mixed reactor model. This can be explained by the presence of filter and drier elements in the sampling system which may cause some smearing. This is consistent with the cut-off frequency of about 2 Hz in the cospectra (Fig. 6).

3.2 CH₄ concentration and fluxes

Time series of the methane mixing ratios during the field campaign are shown in Fig. 5. The CH₄ mole fraction values retrieved by the QCLAS are averaged to 1 min, calibrated and reported in dry air. The comparison of the data sets obtained from the two instruments is illustrated by a scatter plot with the associated histogram of their ratio. The combined effect of water dilution and pressure broadening experienced by the FMA leads to a shifted and broadened distribution profile of the histogram. This is because contrary to the FMA which directly measured CH₄ in humid air samples, the strategy for the QCLAS measurements was to dry the air. Nevertheless, available air humidity measurements at the site allowed for an approximate correction of water effects on the methane mole fraction values measured by the FMA. It is evident that not drying the air only led to about 1% error at most in absolute concentration during the entire field campaign, which is acceptable for most applications.

Field intercomparison

B. Tuzson et al.

Title Page

Abstract

Introduction

Conclusions

References

Tables

Figures

◀

▶

◀

▶

Back

Close

Full Screen / Esc

Printer-friendly Version

Interactive Discussion



**Field
intercomparison**B. Tuzson et al.

[Title Page](#)[Abstract](#)[Introduction](#)[Conclusions](#)[References](#)[Tables](#)[Figures](#)[◀](#)[▶](#)[◀](#)[▶](#)[Back](#)[Close](#)[Full Screen / Esc](#)[Printer-friendly Version](#)[Interactive Discussion](#)

The excellent agreement of both analyzers for mixing ratios does not automatically imply comparable results with respect to flux measurements. Thus, we have also tested whether (i) the sensitivity of the two CH₄ analyzers is sufficient to resolve the artificial flux produced by fumigation from a rectangular surface and (ii) the calculated flux agrees with the flux value estimated based on the applied emission rates.

Figure 6 shows cospectra and power spectra obtained during a period with high artificial CH₄ flux (102 nmol CH₄ m⁻² s⁻¹). Since the two instruments gave very consistent results during the entire field campaign, these spectra can be considered as representative for our setups under stationary turbulence conditions. Contrary to the ideal Kaimal spectra, real spectra show systematic damping in the high frequency part, which must be corrected. For the QCLAS system, an empirical approach described by Ammann et al. (2006) was used. This correction can be parameterized as a function of the wind speed and will be specific to the used set-up. For the FMA system, the correction was derived from the damped cospectra which are approximated by a statistical best fitted theoretical cospectra as suggested by Eugster and Senn (1995). The difference between the two methods was analyzed and quantified by calculating the damping loss correction for the QCLAS with the same approach as for the FMA. This would lead to an average correction reduction of about 6% for the QCLAS EC-system.

The agreement of measured cospectra with the idealized Kaimal cospectra (Kaimal et al., 1972, with minor modifications as shown by Eugster and Senn, 1995) is remarkable for both instruments, despite the larger noise level of the QCLAS (see Fig. 6). It is also noteworthy, that the significantly larger white noise level of the QCLAS does not compromise its performance for flux measurements. This is not unexpected since the eddy covariance method is a random-noise rejection method, that is, because random noise of the CH₄ sensor is uncorrelated with random noise of the wind sensor, the covariances and thus the cospectra are unaffected by pure random noise. What is however clearly seen is the fact that both systems are not perfect at the highest frequencies and the cospectra differ from idealized conditions as expected from first-order damping (Eugster and Senn, 1995).

**Field
intercomparison**

B. Tuzson et al.

Title Page

Abstract

Introduction

Conclusions

References

Tables

Figures

◀

▶

◀

▶

Back

Close

Full Screen / Esc

Printer-friendly Version

Interactive Discussion



The main goal of the fumigation experiment was to investigate whether the EC systems adequately measure the simulated flux. Therefore, the calculated 30-min fluxes were compared to each other as well as against the fumigation flux (see Fig. 7). In order to compare the measured fluxes with the emissions from the fumigation area, the footprint correction according to Neftel et al. (2008) was applied. This correction was calculated for each system individually, as the towers were slightly apart from each other. Periods with less than 20% contribution from the artificial source were not included in further analysis because the uncertainties inherent to the footprint calculation were considered as too large. The agreement between the footprint corrected fluxes and the released trace gas flux is remarkable and even fluctuations in the flux due to changes in wind direction occur simultaneously. Nevertheless, the agreement with the known source is suffering during these conditions, because the sudden shifts in wind direction might not be reflected precisely enough by the footprint calculated with half-hourly averaged micrometeorological quantities. As soon as the wind direction is constant, the scatter of the measured and footprint weighted fluxes is getting very small. The methane flux measured by the QCLAS system was systematically slightly higher than the flux determined based on the FMA measurements. However, the mean difference was $5.9 \text{ nmol CH}_4 \text{ m}^{-2} \text{ s}^{-1}$ and thus well below the uncertainty that one would expect for eddy covariance flux measurements. This is remarkable given that the relevant data includes not only concentration measurements but also all assumptions and procedures used during flux calculation and the relevant footprint simulation.

We also recall that during the field campaign the sample was dried for QCLAS measurements, whereas the FMA was analyzing humid air. Thus, for an unbiased comparison, the methane flux retrieved by the FMA system had to be corrected for density fluctuations (WPL term) as well as for cross-talk effect according the approach of Neftel et al. (2010). For illustration, we calculated term II of Eq. (6) for typical conditions experienced during our experiments. Taking for the water flux $w' \rho'_v = 4 \text{ mmol m}^{-2} \text{ s}^{-1}$, the average methane mixing ratio $[\text{CH}_4] = 2 \text{ ppm}$ (from Fig. 5) and the water effect quantified by the dilution experiment (from Fig. 3), the term II results in a flux of $5.6 \text{ nmol m}^{-2} \text{ s}^{-1}$.

**Field
intercomparison**

B. Tuzson et al.

Title Page

Abstract

Introduction

Conclusions

References

Tables

Figures

◀

▶

◀

▶

Back

Close

Full Screen / Esc

Printer-friendly Version

Interactive Discussion



Ecosystem research will certainly have high benefits of recent developments achieved in infrared laser and detector technologies. This is particularly true for the quantum cascade laser fabrication. The latest cw-QCLs can operate at room-temperature (up to 50° C) and have much higher output power and, thus, they are expected to allow significant improvements in the sensitivity of both direct absorption and cavity enhanced spectroscopy. It is also noteworthy, that the QCLAS used in this study simultaneously detects N₂O and NO₂ with sufficient precision and time resolution for eddy covariance flux measurements. Similarly, the most recent cavity enhanced analyzers include multiple species, e.g. CH₄, CO₂ and H₂O, and perform dilution and line-broadening correction on the retrieved mixing ratio values. Finally, for both QCLAS and FMA, new analyzers capable of carbon isotope specific on-line CH₄ measurement are under development.

Acknowledgements. BT thanks Albert Manninen for sharing the Matlab code to generate absorption spectra which include the water broadening contribution. This study was supported by the COST action 729 project “Assessment of nitrogen biosphere-atmosphere exchange based on novel quantum cascade laser technology” SBF Nr. C06.0017, and by the project MAIOLICA of the ETH Competence Center Environment and Sustainability (CCES).

References

- Ammann, C., Brunner, A., Spirig, C., and Neftel, A.: Technical note: Water vapour concentration and flux measurements with PTR-MS, *Atmos. Chem. Phys.*, 6, 4643–4651, doi:10.5194/acp-6-4643-2006, 2006. 2979
- Ammann, C., Flechard, C. R., Leifeld, J., Neftel, A., and Fuhrer, J.: The carbon budget of newly established temperate grassland depends on management intensity, *Agr. Ecosyst. Environ.*, 121, 5–20, 2007. 2966, 2968
- Baer, D. S., Paul, J. B., Gupta, M., and O’Keefe, A.: Sensitive absorption measurements in the near-infrared region using off-axis integrated-cavity-output spectroscopy, *Appl. Phys. B*, 75, 261–265, 2002. 2966

**Field
intercomparison**

B. Tuzson et al.

[Title Page](#)[Abstract](#)[Introduction](#)[Conclusions](#)[References](#)[Tables](#)[Figures](#)[◀](#)[▶](#)[◀](#)[▶](#)[Back](#)[Close](#)[Full Screen / Esc](#)[Printer-friendly Version](#)[Interactive Discussion](#)

- Bain, W. G., Hutyra, L., Patterson, D. C., Bright, A. V., Daube, B. C., Munger, J. W., and Wofsy, S. C.: Wind-induced error in the measurement of soil respiration using closed dynamic chambers, *Agr. Forest Meteorol.*, 131, 225–232, 2005. 2963
- 5 Bartlett, K. B. and Harriss, R. C.: Review and assessment of methane emissions from wetlands, *Chemosphere*, 261(1–4), 261–320, 1993. 2962
- Bowling, D. R., Miller, J. B., Rhodes, M. E., Burns, S. P., Monson, R. K., and Baer, D.: Soil, plant, and transport influences on methane in a subalpine forest under high ultraviolet irradiance, *Biogeosciences*, 6, 1311–1324, doi:10.5194/bg-6-1311-2009, 2009. 2970
- 10 Brown, L. R., Benner, D. C., Champion, J. P., Devi, V. M., Fejard, L., Gamache, R. R., Gabard, T., Hilico, J. C., Lavorel, B., Loete, M., Mellau, G. C., Nikitin, A., Pine, A. S., Predoi-Cross, A., Rinsland, C. P., Robert, O., Sams, R. L., Smith, M. A. H., Tashkun, S. A., and Tyuterev, V. G.: Methane line parameters in HITRAN, *J. Quant. Spectrosc. Ra.*, 82, 219–238, 2003. 2973
- Bubier, J. L. and Moore, T. R.: An ecological perspective on methane emissions from northern wetlands, *Trends Ecol. Evol.*, 9, 460–464, 1994. 2962
- 15 Camarda, M., Gurrieri, S., and Valenza, M.: Effects of soil gas permeability and recirculation flux on soil CO₂ flux measurements performed using a closed dynamic accumulation chamber, *Chem. Geol.*, 265, 387–393, 2009. 2963
- Chen, H., Winderlich, J., Gerbig, C., Hofer, A., Rella, C. W., Crosson, E. R., Van Pelt, A. D., Steinbach, J., Kolle, O., Beck, V., Daube, B. C., Gottlieb, E. W., Chow, V. Y., Santoni, G. W., and Wofsy, S. C.: High-accuracy continuous airborne measurements of greenhouse gases (CO₂ and CH₄) using the cavity ring-down spectroscopy (CRDS) technique, *Atmos. Meas. Tech.*, 3, 375–386, doi:10.5194/amt-3-375-2010, 2010. 2981
- 20 Eugster, W. and Plüss, P.: A fault-tolerant eddy covariance system for measuring CH₄ fluxes, *Agr. Forest Meteorol.*, 150, 841–851, 2010. 2963, 2969, 2970
- 25 Eugster, W. and Senn, W.: A cospectral correction model for measurement of turbulent NO₂ flux, *Bound.-Lay. Meteorol.*, 74, 321–340, 1995. 2979
- Eugster, W., Zeyer, K., Zeeman, M., Michna, P., Zingg, A., Buchmann, N., and Emmenegger, L.: Methodical study of nitrous oxide eddy covariance measurements using quantum cascade laser spectrometry over a Swiss forest, *Biogeosciences*, 4, 927–939, doi:10.5194/bg-4-927-2007, 2007. 2963
- 30 Fowler, D., Hargreaves, K. J., Skiba, U., Milne, R., Zahniser, M. S., Moncrieff, J. B., Beverland, I. J., Gallagher, M. W., Ineson, P., Garland, J., and Johnson, C.: Measurements of CH₄ and N₂O fluxes at the landscape scale using micrometeorological methods, *Philos T. Roy.*

**Field
intercomparison**

B. Tuzson et al.

[Title Page](#)
[Abstract](#)
[Introduction](#)
[Conclusions](#)
[References](#)
[Tables](#)
[Figures](#)
[◀](#)
[▶](#)
[◀](#)
[▶](#)
[Back](#)
[Close](#)
[Full Screen / Esc](#)
[Printer-friendly Version](#)
[Interactive Discussion](#)


Soc. A, 351, 339–356, 1995. 2963

Friborg, T., Christensen, T., and Søgaard, H.: Rapid response of greenhouse gas emission to early spring thaw in a subarctic mire as shown by micrometeorological techniques, *Geophys. Res. Lett.*, 24, 3061–3064, 1997. 2963

5 Hendriks, D. M. D., Dolman, A. J., van der Molen, M. K., and van Huissteden, J.: A compact and stable eddy covariance set-up for methane measurements using off-axis integrated cavity output spectroscopy, *Atmos. Chem. Phys.*, 8, 431–443, doi:10.5194/acp-8-431-2008, 2008. 2963, 2970

10 Ibrom, A., Dellwik, E., Flyvbjerg, H., Jensen, N. O., and Pilegaard, K.: Strong low-pass filtering effects on water vapour flux measurements with closed-path eddy correlation systems, *Agr. Forest Meteorol.*, 147, 140–156, 2007. 2975

Kaimal, J. C., Wyngaard, J. C., Izumi, Y., and Coté, O. R.: Spectral characteristics of surface-layer turbulence, *Q. J. Roy. Meteorol. Soc.*, 98, 563–589, 1972. 2979

15 Keppler, F., Hamilton, J. T. G., Braß, M., and Röckmann, T.: Methane emissions from terrestrial plants under aerobic conditions, *Nature*, 439, 187–191, 2006. 2976

Kormann, R., Müller, H., and Werle, P.: Eddy flux measurements of methane over the fen “Murnauer Moos”, 11°11′ E, 47°39′ N, using a fast tunable diode laser spectrometer, *Atmos. Environ.*, 35, 2533–2544, 2001. 2967

20 Kroon, P. S., Hensen, A., Jonker, H. J. J., Zahniser, M. S., Van't Veen, W. H., and Vermeulen, A. T.: Suitability of quantum cascade laser spectroscopy for CH₄ and N₂O eddy covariance flux measurements, *Biogeosciences*, 4, 715–728, doi:10.5194/bg-4-715-2007, 2007. 2963, 2970

Matthias, A. D., Yarger, D. N., and Weinbeck, R. S.: A numerical evaluation of chamber methods for determining gas fluxes, *Geophys. Res. Lett.*, 5, 765–768, 1978. 2963

25 McManus, J. B., Nelson, D. D., Herndon, S. C., Shorter, J. H., Zahniser, M. S., Blaser, S., Hvozda, L., Muller, A., Giovannini, M., and Faist, J.: Comparison of cw and pulsed operation with a TE-cooled quantum cascade infrared laser for detection of nitric oxide at 1900 cm⁻¹, *Appl. Phys. B*, 85, 235–241, 2006. 2965

30 Neftel, A., Flechard, C., Ammann, C., Conen, F., Emmenegger, L., and Zeyer, K.: Experimental assessment of N₂O background fluxes in grassland systems, *Tellus B*, 59, 470–482, 2007. 2963

Neftel, A., Spirig, C., and Ammann, C.: Application and test of a simple tool for operational footprint evaluations, *Environ. Pollut.*, 152, 644–652, 2008. 2967, 2980

**Field
intercomparison**

B. Tuzson et al.

[Title Page](#)[Abstract](#)[Introduction](#)[Conclusions](#)[References](#)[Tables](#)[Figures](#)[◀](#)[▶](#)[◀](#)[▶](#)[Back](#)[Close](#)[Full Screen / Esc](#)[Printer-friendly Version](#)[Interactive Discussion](#)

- Neftel, A., Ammann, C., Fischer, C., Spirig, C., Conen, F., Emmenegger, L., Tuzson, B., and Wahlen, S.: N₂O exchange over managed grassland: application of a quantum cascade laser spectrometer for micrometeorological flux measurements, *Agr. Forest Meteorol.*, 150, 775–785, 2010, special Issue on Eddy Covariance (EC) flux measurements of CH₄ and N₂O. 2969, 2973, 2974, 2975, 2976, 2980, 2981
- 5 Nelson, D. D., Shorter, J. H., McManus, J. B., and Zahniser, M. S.: Sub-part-per-billion detection of nitric oxide in air using a thermoelectrically cooled mid-infrared quantum cascade laser spectrometer, *Appl. Phys. B*, 75, 343–350, 2002. 2966
- Rothman, L. S., Gordon, I. E., Barbe, A., et al.: The HITRAN 2008 molecular spectroscopic database, *J. Quant. Spectrosc. Ra.*, 110, 533–572, 2009. 2966
- 10 Smeets, C. J. P. P., Holzinger, R., Vigano, I., Goldstein, A. H., and Röckmann, T.: Eddy covariance methane measurements at a Ponderosa pine plantation in California, *Atmos. Chem. Phys.*, 9, 8365–8375, doi:10.5194/acp-9-8365-2009, 2009. 2963, 2970
- Smith, K. A., Dobbie, K. E., Ball, B. C., Bakken, L. R., Sitaula, B. K., Hansen, S., Brumme, R., Borken, W., Christensen, S., Prieme, A., Fowler, D., Macdonald, J. A., Skiba, U., Klemedtsson, L., Kasimir-Klemedtsson, A., Degorska, A., and Orlanski, P.: Oxidation of atmospheric methane in Northern European soils, comparison with other ecosystems, and uncertainties in the global terrestrial sink, *Glob. Change Biol.*, 6, 791–803, 2000. 2976
- 15 Varghese, P. L. and Hanson, R. K.: Collisional narrowing effects on spectral line shapes measured at high resolution, *Appl. Optics*, 23, 2376–2385, 1984. 2972
- Verma, S. B., Ullman, F. G., Billesbach, D., Clement, R. J., Kim, J., and Verry, E. S.: Eddy correlation measurements of methane flux in a northern peatland ecosystem, *Bound.-Lay. Meteorol.*, 58, 289–304, 1992. 2963
- Webb, E., Pearman, G., and Leuning, R.: Correction of flux measurements for density effects due to heat and water vapour transfer, *Q. J. Roy. Meteorol. Soc.*, 106, 85–100, 1980. 2971, 2975
- 25 Werle, P. and Kormann, R.: Fast chemical sensor for eddy-correlation measurements of methane emissions from rice paddy fields, *Appl. Optics*, 40, 846–858, 2001. 2963
- Werle, P., Mücke, R., and Slemr, F.: The limits of signal averaging in atmospheric trace-gas monitoring by tunable diode-laser absorption spectroscopy (TDLAS), *Appl. Phys. B*, 57, 131–139, 1993. 2969, 2970
- 30

Field
intercomparison

B. Tuzson et al.

Title Page

Abstract

Introduction

Conclusions

References

Tables

Figures

◀

▶

◀

▶

Back

Close

Full Screen / Esc

Printer-friendly Version

Interactive Discussion

**Table 1.** Characteristics of the two EC flux systems and respective analysers.

Parameters	EC system with FMA	EC system with QCLAS
Analyser Type	off-axis integrated cavity output spectrometer	dual cw quantum cascade laser direct absorption spectrometer
Measured species	CH ₄	CH ₄ ; H ₂ O; N ₂ O; NO ₂
CH ₄ absorption line position (μm)	1.65	7.84
CH ₄ line intensity (×10 ⁻²¹ cm ⁻¹ /molecule cm ⁻²)	0.8–1.3 ^a	24.6
Optical path length (m)	3300 < L < 3450 ^b	76
Cell volume (L)	0.4	0.5
Cell pressure (kPa)	19	8
Sonic anemometer type	Gill Instruments R2A (3-D)	Gill Instruments HS (3-D)
Sample line inlet position	0.25 m below sonic center	0.25 m below sonic center
Sonic measurement height (m)	1.2	1.2
Sampling tube length (m)	6.7	25
Sample gas flow at inlet (L min ⁻¹)	30.5	13.5
Selected data acquisition rate (Hz)	20	8

^a There are four closely spaced CH₄ absorption lines, which are not resolved by the FMA.

^b The exact value is not known. The lower limit was estimated based on normal operation condition of the FMA, i.e. measuring ≈2 ppm CH₄ at a cell pressure of 19 kPa results in about 16% absorption signal. This translates in 3.3 km considering the line intensities and assuming no optical loss within the cavity. The upper limit is calculated from the reported cavity ring-down time of 11.6 μs.

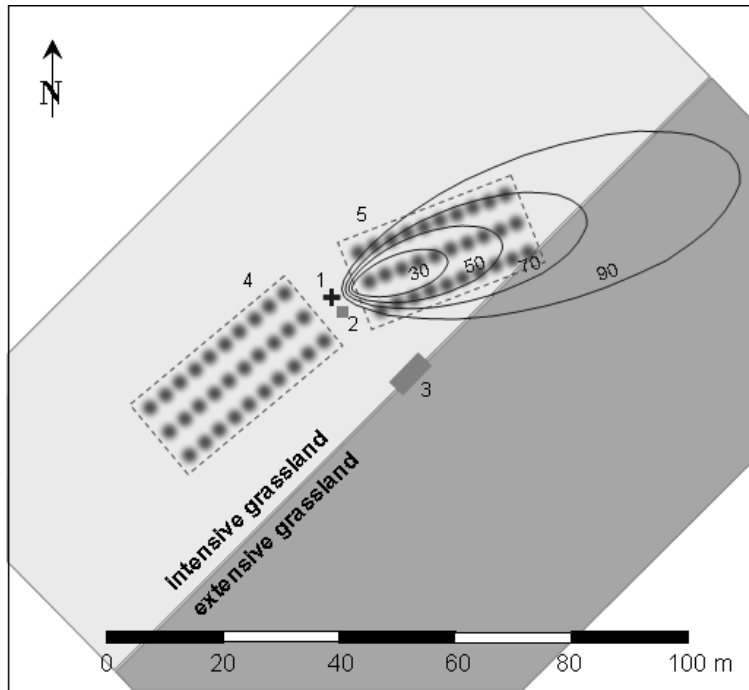


Fig. 1. Schematic map of the experimental field setup. (1) position of both EC flux systems: sonic anemometers and sample tube inlets for QCLAS and FMA; (2) weatherproof housing with the FMA; (3) trailer housing the QCLAS; (4) and (5) alternate positions of fumigation grids for the two main wind directions: circles indicate the position of the 30 release orifices, the dashed enveloping rectangle represents the source area used in the footprint calculation (assuming a constant average emission flux). The contour lines illustrate the flux footprint with 30%, 50%, 70%, and 90% flux contribution for a northeasterly wind case on 31 March 2009 11:00–14:30 CEST ($u=3.8 \text{ m s}^{-1}$, $z/L=-0.1$).

**Field
intercomparison**

B. Tuzson et al.

Title Page

Abstract

Introduction

Conclusions

References

Tables

Figures

⏪

⏩

◀

▶

Back

Close

Full Screen / Esc

Printer-friendly Version

Interactive Discussion



Field
intercomparison

B. Tuzson et al.

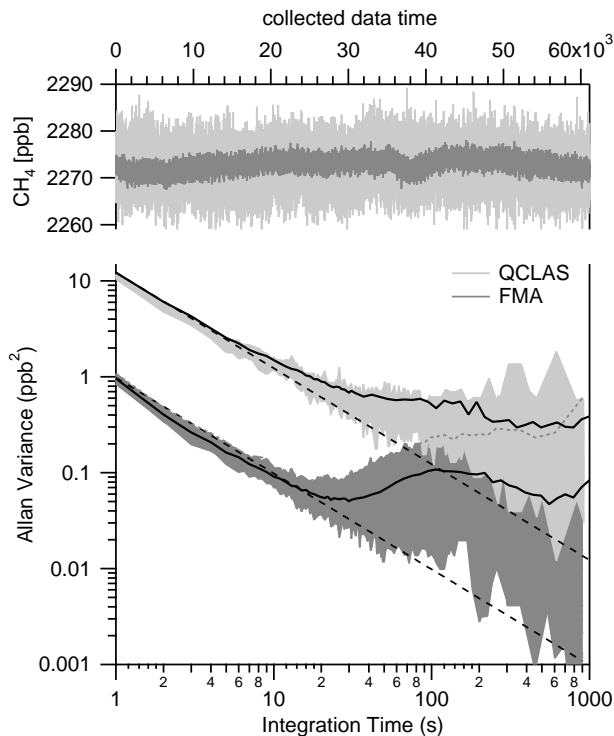


Fig. 2. Precision and long-term stability of both analyzers quantified by the Allan variance technique. The top part shows the CH₄ mixing ratio measured over 16 h by the two analyzers from a pressurized air cylinder. Data from the QCLAS are shown in light gray, those from the FMA are in dark gray. The bottom part is the log-log plot of the sample variance as a function of the averaging time. The dashed line indicates the white-noise behavior, while the black line is the variance associated to the long-term measurement. The time series was also split into 30 min sequences and all individual Allan variance plots were calculated. The filled areas thus represent the envelope of all individual 30 min Allan variance plots, indicating the range that typical 30 min Allan variances would fall into.

[Title Page](#)[Abstract](#)[Introduction](#)[Conclusions](#)[References](#)[Tables](#)[Figures](#)[◀](#)[▶](#)[◀](#)[▶](#)[Back](#)[Close](#)[Full Screen / Esc](#)[Printer-friendly Version](#)[Interactive Discussion](#)

Field
intercomparison

B. Tuzson et al.

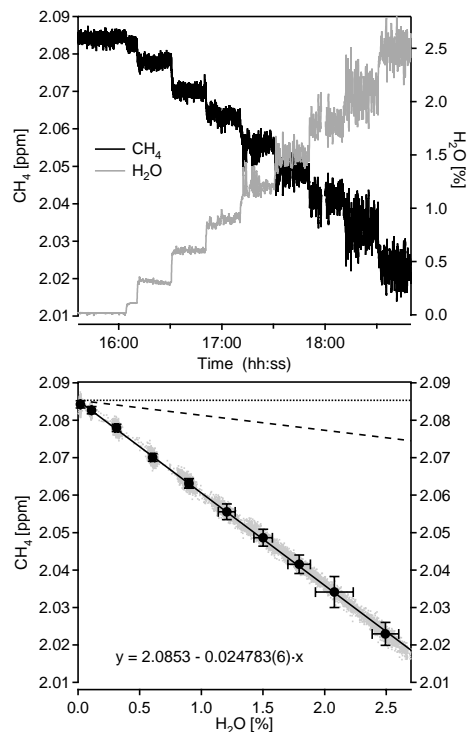


Fig. 3. Instrumental response to varying water vapor content. Top graph shows the methane mixing ratio changes over time induced by the stepwise addition of water vapour. The same behaviour was observed for both analyzers. The linear dependence of the CH₄ mixing ratio on the water vapour concentration as measured by QCLAS is indicated on the bottom graph. The gray dots show the original one-second data while the circles represent 20 min averages (with 1 σ error bars) for the individual dilution steps. The solid line is a linear fit through the averaged data points. The dashed line indicates the apparent CH₄ mixing ratio after correction of the volumetric dilution (Eq. 3) by water vapor. The real (dry air) mixing ratio (dotted line) can only be obtained when an additional correction factor (Eq. 5) is applied to account for the pressure broadening effect.

Title Page

Abstract

Introduction

Conclusions

References

Tables

Figures

◀

▶

◀

▶

Back

Close

Full Screen / Esc

Printer-friendly Version

Interactive Discussion



Field
intercomparison

B. Tuzson et al.

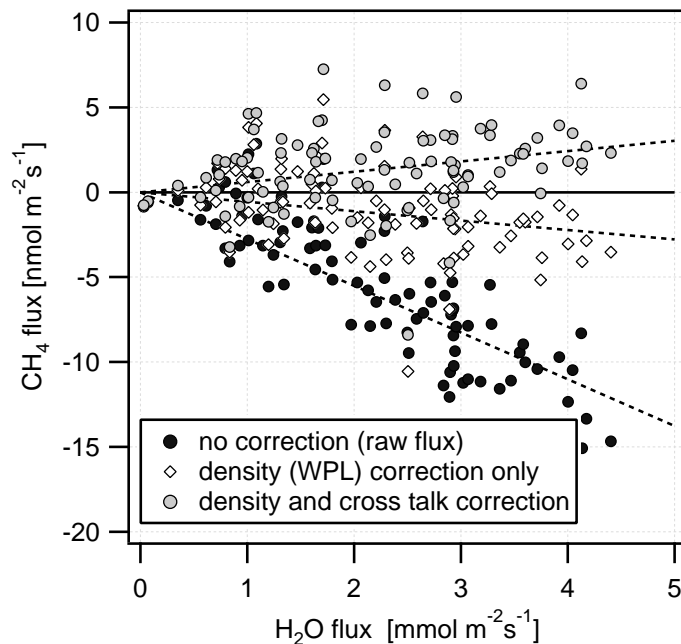


Fig. 4. Scatter plot of the evaluated CH₄ fluxes at different stages of corrections. These data were recorded with the QCLAS at the same site during August 2008 when water fluxes were high and no significant methane fluxes were expected. The dashed lines show linear regression curves (forced through zero) for the three data-sets. The regression line slope for the data with “no correction” is $-2.7 \text{ nmol CH}_4 (\text{mmol H}_2\text{O})^{-1}$.

[Title Page](#)[Abstract](#)[Introduction](#)[Conclusions](#)[References](#)[Tables](#)[Figures](#)[◀](#)[▶](#)[◀](#)[▶](#)[Back](#)[Close](#)[Full Screen / Esc](#)[Printer-friendly Version](#)[Interactive Discussion](#)

Field
intercomparison

B. Tuzson et al.

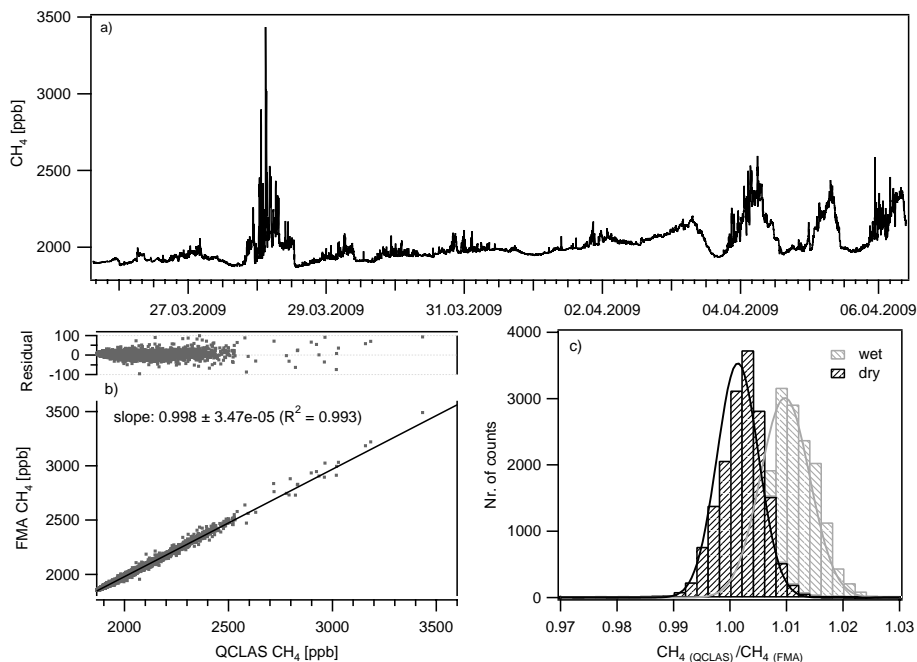


Fig. 5. (a) Time series of the methane mixing ratios during the field campaign. (b) Scatter plot between the data sets measured by QCLAS and FMA, and (c) a histogram plot of the ratio between these two data sets illustrating two situations: the ratio calculated using CH_4 measured by the FMA in humid air (gray bars) and the ratio when the FMA data were dilution corrected (black bars). The appended gaussian fit indicates that the ratio between the two data sets has a nearly normal distribution.

Title Page

Abstract

Introduction

Conclusions

References

Tables

Figures

◀

▶

◀

▶

Back

Close

Full Screen / Esc

Printer-friendly Version

Interactive Discussion



Field
intercomparison

B. Tuzson et al.

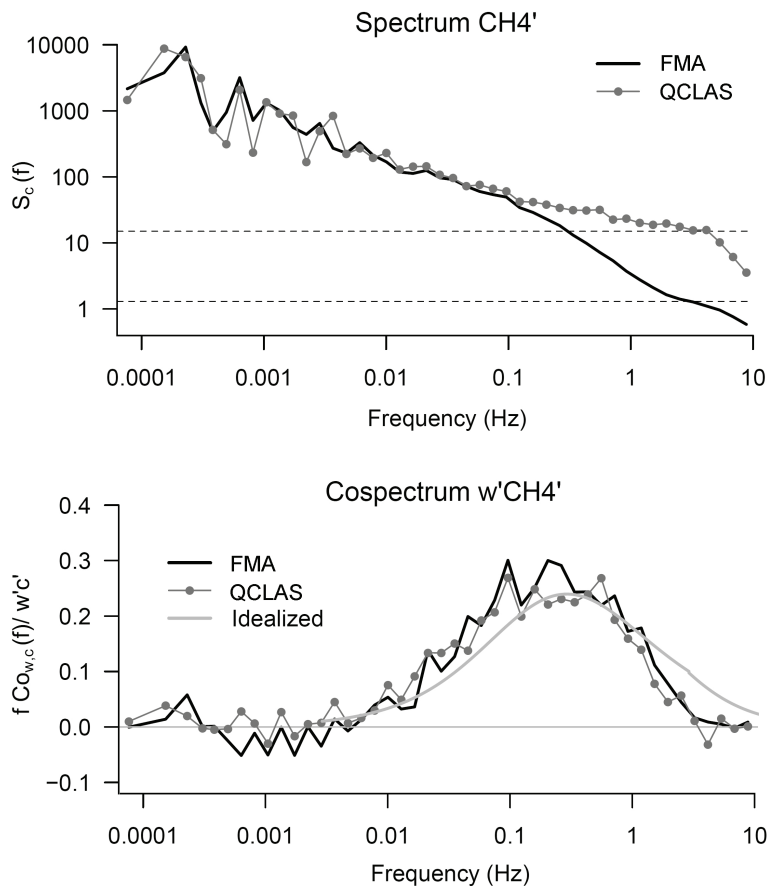


Fig. 6. Comparison of spectra and cospectra during high flux conditions ($102 \text{ nmol CH}_4 \text{ m}^{-2} \text{ s}^{-1}$, 31 March 2009, 11:00–14:38 CEST (218 records) with $u=3.86 \text{ m s}^{-1}$). The gray line shows the idealized cospectrum for neutral and unstable conditions according to Kaimal et al. (1972).

Field
intercomparison

B. Tuzson et al.

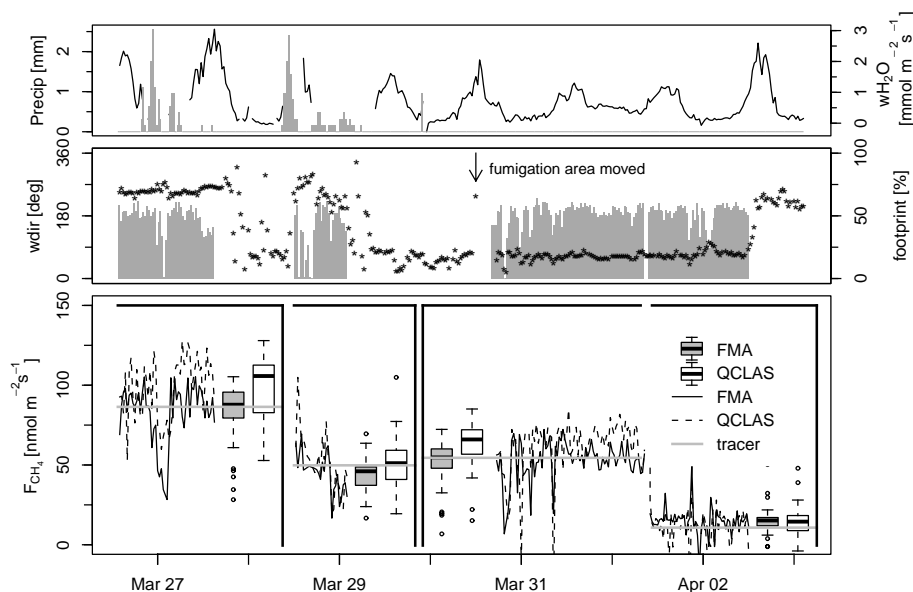


Fig. 7. Methane fluxes during the fumigation experiment. The top panel shows precipitation and the latent energy flux. Wind direction and the proportion of contributed by the fumigated area to the measured flux is displayed in the middle panel. In the lowest panel, the footprint corrected fluxes are plotted. Additionally, a boxplot for each system summarizes the footprint corrected flux for the individual fumigation period. The gray solid line represents the issued flux.

[Title Page](#)[Abstract](#)[Introduction](#)[Conclusions](#)[References](#)[Tables](#)[Figures](#)[◀](#)[▶](#)[◀](#)[▶](#)[Back](#)[Close](#)[Full Screen / Esc](#)[Printer-friendly Version](#)[Interactive Discussion](#)